

A Three-Field (Displacement-Pressure-Concentration) Formulation for Coupled Transport-Deformation Problems

Hao Yan and Caglar Oskay*

Department of Civil and Environmental Engineering
Vanderbilt University
Nashville, TN 37235

Abstract

This manuscript provides a three-field finite element formulation for the evaluation of coupled transport-deformation problems. A stabilized advection-diffusion-reaction model is employed to idealize the mass transport of an aggressive environmental agent within a solid medium, whereas the deformation response of the medium is formulated using the mixed finite element approach with pressure and displacement as unknown variables. The proposed model accurately captures the pressure and pressure gradient fields that characterize the reaction and advection terms of the mass transport model. The concentration-dependent viscoplastic deformation response is idealized using a generalized Johnson-Cook plasticity model. The accuracy characteristics of the proposed three-field formulation are assessed by numerical simulations, which indicate the significance of accurate estimation of pressure at high stress gradient zones for correct characterization of mass transport.

Keywords: Multiphysics; Coupled problems; Multi-field formulation; Environmental effects; Oxygen embrittlement.

1 Introduction

Aggressive environmental elements deteriorate the mechanical performance of material and structural systems subjected to combined loading and environmental conditions. Examples of engineering problems that display environmental-deformation response coupling are manifold. Two problems that have received significant attention, among others, are hydrogen- and oxygen-induced embrittlement in metals [1, 2].

*Corresponding author address: VU Station B#351831, 2301 Vanderbilt Place, Nashville, TN 37235. Email: caglar.oskay@vanderbilt.edu

Predictive computational modeling of the deformation response of such materials and structures subjected to aggressive environmental agents remains to be a significant challenge. The first difficulty is accurately modeling the coupling mechanisms between the inelastic deformation process and the mass transport of the aggressive agent into the structural material. The second difficulty is the development of a computational solution method to accurately evaluate the response in the presence of the coupling mechanisms. An extensive literature exists in characterization and modeling of metals subjected to hydrogen; and to a lesser extent, oxygen. The mass transport of the aggressive agent into the solid substrate is often modeled as a diffusion-advection-reaction problem [3], whereas the mechanical response involves inelastic deformations induced by the mechanical and thermal loads, as well as the environmental effects. Time-dependent deterioration of the mechanical properties is marked by the coupling between the transport process of the aggressive agent and the deformation under mechanical and thermal loads. The transport process typically results in volumetric expansion, hardening, embrittlement, loss of fatigue life and strength [4, 5]. On the other hand, the chemical potential that drives the kinetics of the aggressive agent ingress is a function of the state of stress and deformation through formation of trap sites (e.g., dislocations) and microcracks that enhance the rate of mass transport.

Computational modeling of this phenomenon requires accurate capturing of the coupling effects between the transport and deformation mechanisms. Oskay and Haney [6] proposed a coupled transport-deformation formulation to simulate the oxygen-induced embrittlement of titanium structures. This formulation does not account for the advection-reaction terms that become significant at high stress gradient zones. The seminal work of Sofronis and McMeeking [3] provided the first finite element model for the coupled hydrogen transport - deformation response that can describe the hydrogen transport into a metal substrate around crack tips. This model has been extended to properly account for transport between trap and lattice sites by Krom *et al.* [7]. Ndong-Mefane *et al.* [8] addressed the potential instability problems in advection-dominated transport around crack and notch tips by employing a stabilized finite element approach. The advection coefficient, which depend on the pressure gradient, is typically approximated a-posteriori through discrete differentiation of the pressure estimates at the integration points in a displacement-based finite element solution of the deformation problem. This leads to significant approximation errors at regions of high stress gradients such as notch and crack tips.

In this manuscript, we propose a three-field computational model for the evaluation of coupled transport-deformation problems. The displacement, pressure and concentration fields are evaluated as independent unknowns. The key novel contribution of the present manuscript is the demonstration that the mixed finite element method, in which the pressure is treated as an independent unknown in addition to the displacement degrees of freedom, can be employed to accurately compute the pressure gradient in the deformation problem. The pressure gradient information, in turn, is employed to accurately calculate the instantaneous coefficients of the advection-reaction terms of the mass transport problem. In addition, the computa-

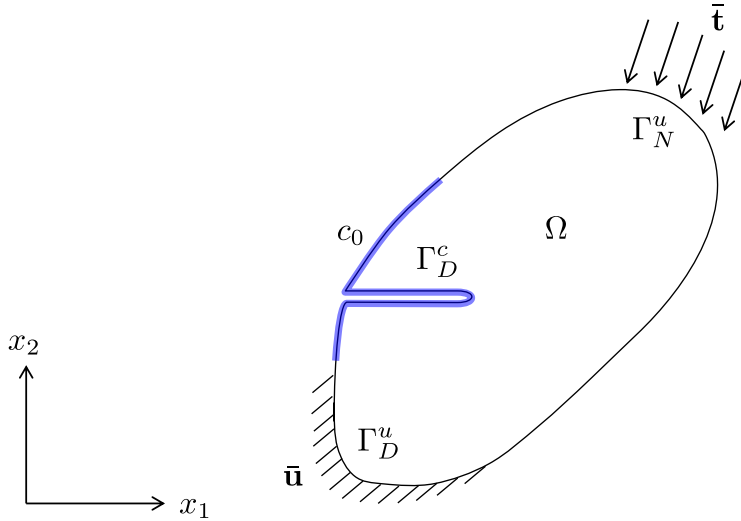


Figure 1: Coupled transport-deformation processes defined on the problem domain, Ω .

tional model has the following properties: (a) the mass transport problem is stabilized to accurately describe the advection-dominated transport in the presence of high stress gradients (e.g., crack and notch tips); (b) the deformation problem is evaluated using a tight-coupled two-field (displacement-pressure) formulation, whereas the transport and deformation processes are evaluated based on a staggered approach to efficiently address problems where the time scales associated with the transport and deformation processes are disparate.

The remainder of the manuscript is organized as follows: Section 2 provides the mass transport model with diffusion-advection-reaction terms coupled to a viscoplasticity model. In Section 3, the finite element model of the coupled physics problems based on the three-field (displacement-pressure-concentration) modeling is described, including the stabilization of the mass transport problem for advection-dominated problems. The details of the implementation of the proposed approach is included. Numerical verification studies to assess the performance of the model in the context of the oxygen ingress problem in titanium alloys are discussed in Section 4. Section 5 provides the conclusions and discussion of future research directions.

2 Problem Statement

Consider the domain of an arbitrary solid body, $\Omega \subset \mathbb{R}^{n_{sd}}$, subjected to an aggressive agent along a part of the domain boundary, $\Gamma = \partial\Omega$, as illustrated in Fig. 1 (n_{sd} : number of space dimensions). When subjected to elevated boundary concentration, fluxes applied on the domain boundary or stress gradient fields, the aggressive agent tends to diffuse into the body. Concurrently, the solid body is subjected to time varying mechanical loading. In this section, the governing equations of the aggressive agent transport and deformation processes are provided, and the coupling mechanisms between the two physical processes are described.

2.1 Transport model

We adopt Oriani's equilibrium theory to describe the diffusion of the aggressive agent into the stressed solid [9]. According to this theory, the driving force for diffusion is due to the chemical potential of the aggressive agent:

$$q_i(\mathbf{x}, t) = -\frac{D(T(\mathbf{x}, t))}{RT(\mathbf{x}, t)} c(\mathbf{x}, t) \mu_{,i}(\mathbf{x}, t) \quad (1)$$

in which, q_i denotes the components of the mass flux; D the diffusivity of the aggressive agent within the solid; T the temperature; R the universal gas constant; μ the chemical potential; and c the concentration of aggressive agent, given as weight ratio of the diffusing agent and the solid substrate within an infinitesimal control volume. We adopt the index notation in the problem formulation (i.e., $i = 1, \dots, n_{\text{sd}}$). Repeated indices of the spatial dimensions indicate summation unless otherwise stated. A subscript followed by a comma indicates partial derivative (i.e., $f_{,i} = \partial f / \partial x_i$). \mathbf{x} and t parameterize the spatial and temporal dimensions, respectively. Bold symbol indicates vector notation (i.e., $\mathbf{x} = [x_1, x_2, x_3]$ for $n_{\text{sd}} = 3$). The chemical potential is a function of the concentration and the state of stress:

$$\mu(\mathbf{x}, t) = \mu_0 + RT \ln(c) - \bar{V}_c p(\mathbf{x}, t) \quad (2)$$

where, μ_0 denotes the chemical potential at the stress free state and at equilibrium concentration; $p = -\sigma_{ii}/3$ denotes the pressure; \bar{V}_c the partial molar volume of the ingressed gas in the substrate solid; and σ_i the components of the stress tensor. Using Eqs. 1 and 2, the transport equation of the stressed solid is given as:

$$\dot{c} - (Dc_{,i})_{,i} - \left(\frac{Dc\bar{V}_c}{RT} p_{,i} \right)_{,i} = 0 \quad (3)$$

with superscribed dot indicates differentiation with respect to time. The initial and boundary conditions for the transport problem are expressed as:

$$c(\mathbf{x}, t = 0) = c_\infty(\mathbf{x}); \quad \mathbf{x} \in \Omega \quad (4)$$

$$c(\mathbf{x}, t) = c_0(\mathbf{x}, t); \quad \mathbf{x} \in \Gamma_D^c \quad (5)$$

$$q_i n_i(\mathbf{x}, t) = 0; \quad \mathbf{x} \in \Gamma_N^c \quad (6)$$

in which, c_∞ is the concentration of the aggressive agent at the natural state of the solid; c_0 the boundary concentration prescribed along $\Gamma_D^c \subset \Gamma$; $\Gamma_D^c \cap \Gamma_N^c = \emptyset$ and $\Gamma_D^c \cup \Gamma_N^c = \Gamma$; and, n_i the components of the unit normal vector. Only homogeneous type Neumann boundary condition is considered for simplicity of the ensuing formulation, but the formulation can be extended to arbitrary Neumann or Robin conditions.

The transport process is coupled to the mechanical deformation through two mechanisms. The first is the stress dependent chemical potential of the aggressive agent, which leads to the

third term in the transport equation (Eq. 3). The second is by linking the diffusivity to the state of damage within the solid. The effect of microcracking and damage on diffusivity has been recognized in geological materials, concrete and metals (e.g., [10–12]). The diffusivity is assumed to be enhanced as a function of the defect density (e.g. microcrack) as proposed by Krajcinovic [12]. The effect of evolving defect density on diffusivity is modeled based on the percolation theory [6] as:

$$D(\omega, T) = D_0 (1 + \mathcal{D}(\omega)) \exp\left(-\frac{Q}{RT}\right) \quad (7)$$

where, D_0 is the pre-exponential constant; Q is the activation energy; and, $\mathcal{D}(\omega)$ the effect of mechanical damage on diffusivity:

$$\mathcal{D}(\omega) = \begin{cases} a\omega; & \omega < \omega_c \\ a\omega - \frac{(\omega - \omega_c)^2}{\omega - \omega_{ec}}; & \omega_c \leq \omega < \omega_{ec} \\ \infty; & \omega \geq \omega_{ec} \end{cases} \quad (8)$$

in which, $\omega \in [0, 1)$ denotes the state of damage at a material point, with $\omega=0$ indicating undamaged state of the material, and, $\omega=1$ corresponds to loss of load carrying capacity at the material point. ω evolves as a function of mechanical loading as described below. ω_c and ω_{ec} denote the conduction and elastic percolation thresholds respectively; and, a is a material parameter.

In the absence of loading induced defect formation, Eq. 7 reduces to the classical Arrhenius form, where the diffusivity varies as a function of temperature only. At low levels of damage ($\omega < \omega_c$), the diffusivity is linearly proportional to the damage variable [11]. When damage exceeds the elastic percolation threshold, a continuous path forms across the material point, permitting free flow of the aggressive agent. At intermediate values of the damage state, the rate of change of diffusivity progressively increases as a function of damage. The idea of using percolation thresholds to relate microcrack networks to transport properties in metals have been previously proposed [13]. In contrast, detailed experimental investigations of damage dependent change in diffusivity in metals has been relatively scarce. Additional experimental investigations would shed further light on the effect of this coupling mechanism.

When the body is subjected to a uniform stress field, the transport process (Eq. 3) reduces to the Fick's law of diffusion, and the state of mechanical deformation affects the diffusion of the aggressive agent through the damage dependent diffusivity only. In the presence of stress gradients induced by crack tips, notches and thermal gradients, pressure significantly affects transport.

2.2 Deformation model

The governing equilibrium equations describing the mechanical response are:

$$\sigma_{ij,j}(\mathbf{x}, t) + b_i(\mathbf{x}, t) = 0 \quad (9)$$

where, b_i is the body force per unit volume. The constitutive response of the body is modeled in the rate form based on the assumption of additive split of the strain field:

$$\dot{\sigma}_{ij} = L_{ijkl} \dot{\varepsilon}_{kl}^e(\mathbf{x}, t) = L_{ijkl} (\dot{\varepsilon}_{kl}(\mathbf{x}, t) - \dot{\mu}_{kl}(\mathbf{x}, t)) \quad (10)$$

in which, ε_{ij} , ε_{ij}^e and μ_{ij} denote the components of total, elastic and inelastic strain tensors, respectively. Assuming small strain kinematics:

$$\varepsilon_{ij} = \frac{1}{2} (u_{i,j}(\mathbf{x}, t) + u_{j,i}(\mathbf{x}, t)) \quad (11)$$

where, u_i denote the components of the displacement field. L_{ijkl} is the fourth order tensor of elastic moduli taken to be symmetric and strongly elliptic:

$$L_{ijkl} = L_{klij} = L_{jikl} = L_{ijlk} \quad (12)$$

$$\zeta_{ij} L_{ijkl} \zeta_{kl} \geq \eta \zeta_{ij} \zeta_{ij}; \quad \forall \zeta_{ij} = \zeta_{ji}; \quad \eta > 0 \quad (13)$$

The inelastic strains, μ_{ij} , is due to the viscoplastic deformation, as well as the lattice strains induced by elevated temperature and aggressive agent content within the lattice:

$$\mu_{ij} = \varepsilon_{ij}^{vp} + \varepsilon_{ij}^T + \varepsilon_{ij}^c \quad (14)$$

where, ε_{ij}^{vp} , ε_{ij}^T and ε_{ij}^c are the viscoplastic, thermal and concentration strains, respectively. Thermal and concentration strains are taken to be volumetric:

$$\varepsilon_{ij}^T = \alpha (T - T_0) \delta_{ij} \quad (15)$$

$$\varepsilon_{ij}^c = \vartheta (c - c_\infty) \delta_{ij} \quad (16)$$

where, δ is second order identity tensor; T_0 is the reference (i.e., room) temperature; α the thermal expansion coefficient; and, ϑ the concentration induced volumetric expansion coefficient. The viscoplastic strain is taken to remain in the deviatoric strain space (i.e., $\varepsilon_{ii}^{vp} = 0$).

Splitting the stress tensor into hydrostatic and deviatoric components and considering the constitutive equations yield:

$$\dot{p} = -\frac{1}{3} \dot{\sigma}_{ii} = -\frac{1}{3} L_{iikl} (\dot{\varepsilon}_{kl} - \dot{\mu}_{kl}) \quad (17)$$

$$\dot{s}_{ij} = \dot{\sigma}_{ij} + p \delta_{ij} = L'_{ijkl} (\dot{\varepsilon}_{kl} - \dot{\mu}_{kl}) \quad (18)$$

where,

$$L'_{ijkl} = L_{ijkl} - \frac{1}{3}L_{nnkl}\delta_{ij} \quad (19)$$

Remark: In this manuscript, the focus is on the response of an isotropic solid. The tensor of elastic moduli then takes the form:

$$L_{ijkl} = k\delta_{ij}\delta_{kl} + 2G \left(\delta_{ik}\delta_{jl} - \frac{1}{3}\delta_{ij}\delta_{kl} \right) \quad (20)$$

where, k and G are bulk and shear moduli, respectively. The pressure is expressed as:

$$p = -ku_{i,i} + 3k[\alpha(T - T_0) + \vartheta(c - c_\infty)] \quad (21)$$

Equation (21) is provided in the total form, since the pressure is independent of viscous and history-dependent effects. The deviatoric part of the elastic moduli is expressed as:

$$L'_{ijkl} = 2G \left(\delta_{ik}\delta_{jl} - \frac{1}{3}\delta_{ij}\delta_{kl} \right) \quad (22)$$

Applying the stress decomposition to the governing equation yields:

$$s_{ij,j}(\mathbf{x}, t) - p_{,i}(\mathbf{x}, t) + b_i(\mathbf{x}, t) = 0 \quad (23)$$

The following boundary conditions are prescribed to evaluate the mechanical problem:

$$u_i(\mathbf{x}, t) = \bar{u}_i(\mathbf{x}, t) \quad \mathbf{x} \in \Gamma_D^u \quad (24)$$

$$\sigma_{ij}n_j = \bar{t}_i(\mathbf{x}, t) \quad \mathbf{x} \in \Gamma_N^u \quad (25)$$

where, \bar{u}_i is the prescribed displacement along the Dirichlet boundary Γ_D^u , \bar{t}_i is the prescribed traction along the Neumann boundary Γ_N^u , such that $\Gamma_D^u \cap \Gamma_N^u = \emptyset$ and $\Gamma_D^u \cup \Gamma_N^u = \Gamma$.

The evolution of the viscoplastic strain is modeled by a generalization of the Johnson-Cook plasticity model. The viscoplastic model employed in this study accounts for the effects of embrittlement and hardening as a function of the aggressive agent concentration [6]. The flow of the viscoplastic strain is expressed in terms of a power law:

$$\dot{\varepsilon}_{ij}^{vp} = \gamma \left\langle \frac{f}{\sigma_Y} \right\rangle^q \frac{\partial f}{\partial \sigma_{ij}} \quad (26)$$

where, γ and q denote fluidity and viscoplastic hardening parameters, respectively; $\langle \cdot \rangle$ denotes Macaulay brackets (i.e., $\langle \cdot \rangle = ((\cdot) + |\cdot|)/2$); σ_Y the flow stress; and, $f(\boldsymbol{\sigma}, \sigma_Y)$ the yield function. The Von-Mises yield function is adopted in this study:

$$f(\sigma_{ij}, \sigma_Y) = \sqrt{3\bar{s}} - \sigma_Y \quad (27)$$

where, \bar{s} is the second invariant of the deviatoric stress, \mathbf{s} . The generalized Johnson-Cook flow stress provides a functional relationship between yielding and the strain, temperature and concentration:

$$\sigma_Y = [A + B (\bar{\varepsilon}^{\nu p})^n + F (c - c_\infty)] [1 - (T^*)^m] \quad (28)$$

in which A , B , F , m and n are material parameters. The effective viscoplastic strain $\bar{\varepsilon}^{\nu p}$ and the non-dimensional temperature T^* are defined as:

$$\bar{\varepsilon}^{\nu p} = \sqrt{\frac{2}{3} \bar{\varepsilon}_{ij}^{\nu p} : \bar{\varepsilon}_{ij}^{\nu p}} \quad (29)$$

$$T^* = \frac{T - T_0}{T_{\text{melt}} - T_0} \quad (30)$$

where, T_{melt} denotes melting temperature of the solid.

The damage progression within the material is modeled as a function of temperature and concentration. Let the damage parameter, ω , be the ratio between the equivalent strain, $\bar{\varepsilon}^{\nu p}$ and the failure strain, ε_f :

$$\omega = \frac{\bar{\varepsilon}^{\nu p}}{\varepsilon_f} \quad (31)$$

where, the failure strain is described as:

$$\varepsilon_f = D_1 (c) (1 + D_5 T^*) \quad (32)$$

in which, D_5 parameterizes the effect of temperature on the failure strain. D_1 varies as a function of concentration and idealize the progressive embrittlement due to aggressive agent ingress:

$$D_1 (c) = \begin{cases} D_1^\infty & \text{if } c \leq c_\infty \\ \frac{1}{c_\infty - c_{\text{crit}}} ((D_1^\infty - D_1^\alpha) c + D_1^\alpha c_\infty - D_1^\infty c_{\text{crit}}) & \text{if } c_\infty < c < c_{\text{crit}} \\ D_1^\alpha & \text{if } c \geq c_{\text{crit}} \end{cases} \quad (33)$$

D_1^∞ denotes the failure strain at room temperature in the absence of elevated concentration; D_1^α denotes failure strain beyond a critical concentration, c_{crit} ; and the embrittlement is assumed to be linear at intermediate concentration values. The effect of aggressive agent ingress on the mechanical response is modeled based on the concentration dependent terms in Eq. 28 and Eq. 33. In Eq. 28, the flow stress is affected by the concentration. Elevated concentration tends to harden the material. In addition to hardening, the elevated concentration embrittles the response by reducing the failure strain in Eq. 32.

3 Finite Element Formulation

In this section, we provide the finite element formulation of the coupled transport and deformation problems. The formulation of the transport process includes the stabilization for the advection dominated flow, whereas the formulation of the deformation is conducted using a mixed (pressure-deformation) approach.

3.1 Weak forms

The governing equation of the aggressive agent transport is viewed as an advection-reaction-diffusion problem of the form:

$$\dot{c} - (Dc_{,i})_{,i} + \alpha_i c_{,i} + \beta c = 0 \quad (34)$$

in which, α_i and β are coefficients of advection and reaction, respectively:

$$\alpha_i = -\frac{D\bar{V}_c}{RT} p_{,i} \quad (35)$$

$$\beta = \left(\frac{D\bar{V}_c T_{,i}}{RT^2} - \frac{D_{,i}\bar{V}_c}{RT} \right) p_{,i} - \frac{D\bar{V}_c}{RT} p_{,ii} \quad (36)$$

It is well known that the numerical evaluation of the advection-reaction-diffusion problem using standard low-order finite elements leads to poor approximation and instability when the flow is dominated by advection or reaction. Considerable literature exists on stabilization approaches for this problem, as explained in [14] and references therein. In this study, we employ the Stabilized Finite Element Method (SFEM) proposed by Franca *et al.* [15] to eliminate potential instabilities. The transport response may be dominated by the advection term around notches and crack tips where high stress gradients are present. In contrast, the amplitude of the pressure Laplacian around the notch tips is typically smaller in magnitude. When the temperature and concentration gradients can be taken to be small (e.g., isothermal conditions and mild variation of diffusivity with respect to concentration), the reaction component is not dominant and stabilization is applied to the advection term only.

Let $\nu \in H_0^1(\Omega)$ be a test function; $H^1(\Omega)$ the Sobolev space of functions with square integrable values and derivatives defined on Ω ; and, $H_0^1(\Omega)$ the subspace of functions in $H^1(\Omega)$ that are homogeneous along the domain boundary, Γ_D^c . The weak form of the transport problem is expressed as:

$$\int_{\Omega} \nu \dot{c} d\Omega + \int_{\Omega} \nu_{,i} Dc_{,i} d\Omega + \int_{\Omega} \nu \alpha_i c_{,i} d\Omega + \int_{\Omega} \nu \beta c d\Omega = 0; \quad \forall \nu \in H_0^1(\Omega) \quad (37)$$

in which, the solution is sought within the solution space: $c \in \mathcal{W}$

$$\mathcal{W} := \{ \hat{c} \in H^1(\Omega) \mid \hat{c} = c_0 \text{ on } \mathbf{x} \in \Gamma_D^c \} \quad (38)$$

with sufficient continuity and smoothness assumed for the functions. Restricting the search for the solution within a finite dimensional subspace based on the Bubnov-Galerkin method, the stabilized finite element formulation is expressed as:

$$\int_{\Omega} \nu^h \dot{c}^h d\Omega + \int_{\Omega} \nu_{,i}^h D c_{,i}^h d\Omega + \int_{\Omega} \nu^h \alpha_i c_{,i}^h d\Omega + \int_{\Omega} \nu^h \beta c^h d\Omega - \sum_{e=1}^{n_{el}} \left[\int_{\Omega_e} \left\{ c^h - \left(D c_{,i}^h \right)_{,i} + \alpha_i c_{,i}^h \right\} \tau_e \left\{ - \left(D \nu_{,i}^h \right)_{,i} + \alpha_i \nu_{,i}^h \right\} d\Omega \right] = 0 \quad (39)$$

in which, $\nu^h \in \mathcal{V}^h \subset H_0^1(\Omega)$ and $c^h \in \mathcal{W}^h \subset \mathcal{W}$ are the test and trial functions belonging to the pertinent finite dimensional subspaces, Ω_e is the domain of the element, e , in a finite element discretization of the problem domain; n_{el} the total number of elements, and τ_e is a stability parameter which varies from element to element. At each element, τ_e is computed based on the following equations:

$$\tau_e = \frac{h_e^2}{\frac{2D}{m_e} [1 + \xi(P_e(x))]} \quad (40)$$

$$P_e(x) = \frac{m_e \|\boldsymbol{\alpha}\|_p h_e}{D} \quad (41)$$

$$\xi(x) = \begin{cases} 1; & 0 \leq x < 1 \\ x; & 1 \leq x \end{cases} \quad (42)$$

where, $m_e=1/3$ and $m_e=1/24$ for linear and quadratic elements, respectively; h_e is the average nodal distance in element, e ; and P_e the Peclet number. Substituting the coefficient of reaction and advection (Eqs. 35 and 36) into Eq. 39 yields:

$$\int_{\Omega} \nu^h \dot{c}^h d\Omega + \int_{\Omega} \nu_{,i}^h D c_{,i}^h d\Omega - \int_{\Omega} \nu^h \left[\frac{D \bar{V}_c}{RT} p_{,ii} + \left(\frac{D \bar{V}_c}{RT} \right)_{,i} p_{,i} \right] c^h d\Omega - \int_{\Omega} \nu^h \frac{D \bar{V}_c}{RT} p_{,i} c_{,i}^h d\Omega - \sum_{e=1}^{n_{el}} \int_{\Omega_e} \left\{ c^h - \left(D c_{,i}^h \right)_{,i} - \frac{D \bar{V}_c}{RT} p_{,i} c_{,i}^h \right\} \tau_e \left\{ - \left(D \nu_{,i}^h \right)_{,i} - \frac{D \bar{V}_c}{RT} p_{,i} \nu_{,i}^h \right\} d\Omega = 0 \quad (43)$$

In the current study, we employ first order (i.e., bilinear for 2-D and trilinear for 3-D) finite elements to discretize the concentration field. The second derivative terms of the concentration field and the test functions in Eq. 43, therefore, vanish. We further assume that the intra-element variation in the coefficients remains small. The pressure field is evaluated as a solution to the deformation problem as defined below and itself is approximated using low-order finite elements. However, assuming vanishing of the term that involve the second derivatives of pressure leads to the partial loss of the reaction component, and the resulting formulation cannot adequately predict self-equilibration of concentrations induced by the pressure gradients. To alleviate this problem, we apply the divergence theorem to the pressure-dependent terms in

Eq. 43:

$$\begin{aligned} \int_{\Omega} \nu^h \left[\frac{D\bar{V}_c}{RT} p_{,ii} + \left(\frac{D\bar{V}_c}{RT} \right)_{,i} p_{,i} \right] c^h d\Omega + \int_{\Omega} \nu^h \frac{D\bar{V}_c}{RT} p_{,i} c_{,i}^h d\Omega \\ = \int_{\Gamma_N^c} \nu^h \frac{D\bar{V}_c}{RT} p_{,i} c^h n_i d\Gamma - \int_{\Omega} \nu_{,i}^h \frac{D\bar{V}_c}{RT} p_{,i} c^h d\Omega \end{aligned} \quad (44)$$

Substituting Eq. 44 to Eq. 43, the following weak form is obtained for the transport problem:

$$\begin{aligned} \int_{\Omega} \nu^h \dot{c}^h d\Omega + \int_{\Omega} \nu_{,i}^h D c_{,i}^h d\Omega + \int_{\Omega} \nu_{,i}^h \frac{D\bar{V}_c}{RT} p_{,i} c^h d\Omega - \int_{\Gamma_N^c} \nu^h \frac{D\bar{V}_c}{RT} p_{,i} c^h n_i d\Gamma \\ + \sum_{e=1}^{n_{el}} \left[\int_{\Omega_e} \nu_{,i}^h \left(\dot{c}^h - D_{,j} c_{,j}^h - \frac{D\bar{V}_c}{RT} p_{,j} c_{,j}^h \right) \tau_e \left(D_{,i} + \frac{D\bar{V}_c}{RT} p_{,i} \right) d\Omega \right] = 0 \end{aligned} \quad (45)$$

The components of Eq. 43 that contains the concentration Laplacian is not included above since for low order finite elements, the concentration Laplacian vanishes. The evaluation of the transport problem clearly requires the computation of the pressure gradient fields. To provide consistent and accurate pressure distribution, the deformation problem is evaluated using a mixed formulation, where the cardinal unknowns are the displacements and the pressure. In this manuscript, the formulation for the mixed finite element approach is presented for an isotropic solid.

Let v_i and q be the test functions for displacement and pressure in the appropriate Sobolev spaces and with sufficient smoothness, and v_i^h and q^h belong to the corresponding finite dimensional subspaces of the test functions v_i and q , respectively. Starting from Eqs. 23 and 21, the weak form of the governing equations of equilibrium are: Find $\mathbf{u}^h \in \mathcal{H}^h \subset \mathcal{H}$ and $p^h \in \mathcal{P}^h \subset H^0(\Omega)$ such that for all ν^h and q^h :

$$\int_{\Omega} \nu_{i,j}^h s_{ij} d\Omega - \int_{\Omega} \nu_{i,i}^h p d\Omega - \int_{\Gamma_N^u} \nu_i^h \bar{t}_i d\Gamma - \int_{\Omega} \nu_i^h b_i d\Omega = 0 \quad (46)$$

$$\int_{\Omega} \frac{1}{k} q^h p^h d\Omega + \int_{\Omega} q^h u_{i,i}^h d\Omega - \int_{\Omega} 3q^h [\alpha (T - T_0) + \vartheta (c - c_{\infty})] d\Omega = 0 \quad (47)$$

in which,

$$\mathcal{H} := \{ \hat{\mathbf{u}} \in [H^1(\Omega)]^{n_{sd}} \mid \hat{\mathbf{u}} = \bar{\mathbf{u}} \text{ on } \mathbf{x} \in \Gamma_D^u \} \quad (48)$$

and, $H^0(\Omega)$ is the space of functions with square integrable values defined on Ω .

3.2 Discretization

Consider a Galerkin discretization of the concentration, displacement and pressure fields:

$$c^h(\mathbf{x}, t) = \sum_{a=1}^{n_c} N_a^c(\mathbf{x}) \hat{c}_a(t) \quad (49)$$

$$u_i^h(\mathbf{x}, t) = \sum_{a=1}^{n_u} N_a^u(\mathbf{x}) \hat{u}_{ai}(t) \quad (50)$$

$$p^h(\mathbf{x}, t) = \sum_{a=1}^{n_p} N_a^p(\mathbf{x}) \hat{p}_a(t) \quad (51)$$

where N_a^c , N_a^u and N_a^p are the basis functions of the concentration, displacement and pressure fields, respectively; $(\hat{\cdot})$ denotes the nodal coefficients of the corresponding field; and, the discretization of the test functions follow the Galerkin method. Substituting the concentration discretization (Eq. 49) into the weak form of the transport equation (i.e., Eq. 45), yields:

$$\begin{aligned} F_b = \sum_{a=1}^{n_c} \left[\int_{\Omega} N_b^c N_a^c d\Omega \dot{\hat{c}}_a + \int_{\Omega} N_{b,i}^c D N_{a,i}^c d\Omega \hat{c}_a + \int_{\Omega} N_{b,i}^c \frac{D\bar{V}_c}{RT} N_{a,p,i}^c d\Omega \hat{c}_a - \right. \\ \left. \int_{\Gamma_N^c} N_b^c \frac{D\bar{V}_c}{RT} N_{a,p,i}^c n_i d\Gamma \hat{c}_a + \sum_{e=1}^{n_{el}} \int_{\Omega_e} N_{b,i}^c \left(N_a^c \dot{\hat{c}}_a(t) - D_{,j} N_{a,j}^c \hat{c}_a - \frac{D\bar{V}_c}{RT} p_{,j} N_{a,j}^c \hat{c}_a \right) \times \right. \\ \left. \times \tau_e \left(D_{,i} + \frac{D\bar{V}_c}{RT} p_{,i} \right) d\Omega \right] = 0; \quad b = 1, \dots, n_c \quad (52) \end{aligned}$$

in which, the pressure gradient term is approximated by the discretization of the pressure field:

$$p_{,i} = \sum_{a=1}^{n_p} N_{a,i}^p(\mathbf{x}) \hat{p}_a(t) \quad (53)$$

Substituting Eqs. 49 and 50 into Eqs. 46 and 47 respectively, the equilibrium equations yield:

$$\begin{aligned} \Psi_{bi} := \int_{\Omega} N_{b,j}^u s_{ij} d\Omega - \sum_{c=1}^{n_p} \int_{\Omega} N_{b,i}^u N_c^p d\Omega \hat{p}_c - \int_{\Gamma_N^u} N_b^u \bar{t}_i d\Gamma \\ - \int_{\Omega} N_b^u b_i d\Omega = 0; \quad b = 1, \dots, n_u \quad \text{and} \quad i = 1, \dots, n_{sd} \quad (54) \end{aligned}$$

$$\begin{aligned} \Theta_c := \sum_{a=1}^{n_p} \int_{\Omega} \frac{1}{k} N_c^p N_a^p d\Omega \hat{p}_a + \sum_{b=1}^{n_u} \int_{\Omega} N_c^p N_{b,i}^u d\Omega \hat{u}_{bi} \\ - \int_{\Omega} 3N_c^p [\alpha(T - T_0) + \vartheta(c - c_{\infty})] d\Omega = 0; \quad c = 1, \dots, n_p \quad (55) \end{aligned}$$

where, the concentration field is computed using Eq. 49. Combining Eqs. 18 and 50 yields:

$$R_{ij} := \dot{s}_{ij} - L'_{ijkl} \left(\sum_{a=1}^{n_u} N_{a,l}^u \dot{\hat{u}}_{ak} \right) + 2G\dot{\epsilon}_{ij}^{vp} = 0 \quad (56)$$

3.3 Numerical implementation

Equations 52, 54-56 constitute a coupled system of nonlinear equations, which are evaluated using the commercial computer program, Diffpack. Diffpack is an object oriented development framework with a library of C++ classes for solution of partial differential equations [16]. It is possible to solve this system of equations such that the unknown coefficients of concentration, displacement and pressure are evaluated simultaneously, or based on the staggered solution approach, in which the evolution of transport and deformation problems are evaluated separately but in a staggered manner. In this study, we consider the physical problems, where the characteristic time scales associated with the transport and mechanical processes are disparate. Typically, the ingress of the aggressive agent is a long-time phenomenon, whereas the mechanical loading is applied in a shorter time scale. Conversely, it is also of interest to investigate the transport response under constant amplitude loading, where the transport is regarded as the fast time scale phenomena. The staggered solution strategy (of isothermal type) is appropriate for such problems that involve disparate time scales, and is adopted in this study. The solution strategy is schematically illustrated in Fig. 2. A manager class controls the execution of the algorithm. At each time step, the mechanical and transport solver classes are invoked to solve the problems in turn until convergence is achieved between the solutions of both problems. The thermal state of the system is provided as an input to both transport and mechanical solvers. In the evaluation of the transport problem, the pressure and the pressure gradients are treated as known fields. The pressure and pressure gradients are computed in the deformation problem as described below. It is well known that the staggered solution algorithm is linearly convergent and unstable for systems with comparable characteristic times. In this study, the investigations are limited to temporally disparate problems only and no instabilities were observed. The transport problem is linear and the numerical implementation is standard. In the remainder of this section, the nonlinear solution procedure for the deformation problem is provided.

3.3.1 Deformation model

The deformation response is evaluated by simultaneously solving Eqs. 54-56. We start by discretizing the evolution equation of the deviatoric stress, which is an ordinary differential equation, using the θ -method:

$$R_{ij} = \Delta s_{ij} - L'_{ijkl} \left(\sum_{a=1}^{n_u} N_{a,l}^u \Delta \hat{u}_{ak} \right) + 2G_{t+\Delta t} \dot{\epsilon}_{ij}^{vp} \theta \Delta t + 2G_t \dot{\epsilon}_{ij}^{vp} (1 - \theta) \Delta t = 0 \quad (57)$$

where $\Delta(\cdot) = {}_{t+\Delta t}(\cdot) - {}_t(\cdot)$, and $\theta \in [0, 1)$ is an algorithmic parameter. $\theta=0, 0.5$ and 1 correspond to forward Euler, midpoint and backward Euler algorithms, respectively. By employing the first order Taylor series expansion of Eqs. 54, 55 and 57 and using the Newton-Raphson method

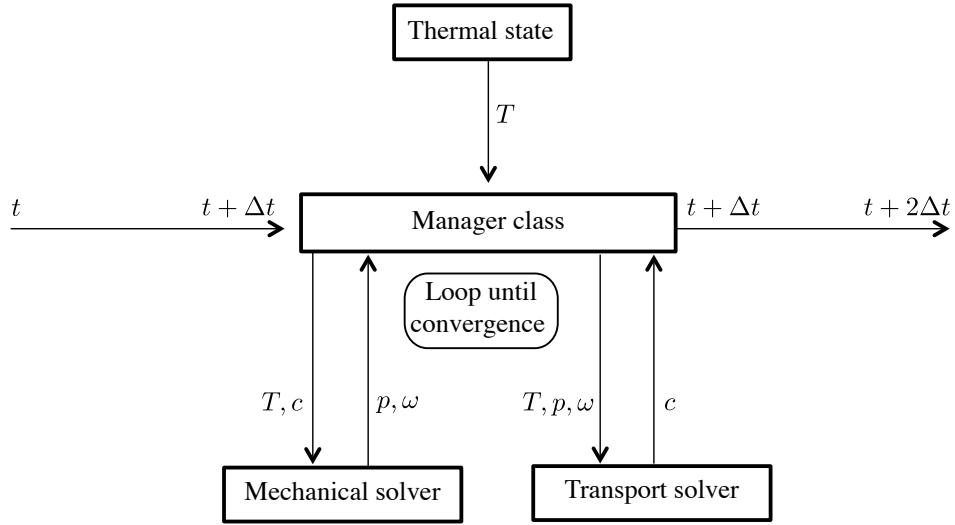


Figure 2: The solution strategy for coupled transport and deformation problems.

yields:

$$\begin{aligned}
{}^{k+1}\Psi_{bi} &\approx {}^k\Psi_{bi} + \left(\frac{\partial\Psi_{bi}}{\partial s_{kl}}\right)^{k+1}\delta s_{kl} + \sum_{c=1}^{n_p} \left(\frac{\partial\Psi_{bi}}{\partial \hat{p}_c}\right)^{k+1}\delta \hat{p}_c \\
&= {}^k\Psi_{bi} + \int_{\Omega} N_{b,j}^u {}^{k+1}\delta s_{ij} d\Omega - \sum_{c=1}^{n_p} \int_{\Omega} N_{b,i}^u N_c^p d\Omega {}^{k+1}\delta \hat{p}_c = 0
\end{aligned} \tag{58}$$

$$\begin{aligned}
{}^{k+1}\Theta_c &\approx {}^k\Theta_c + \sum_{b=1}^{n_u} \left(\frac{\partial\Theta_c}{\partial \hat{u}_{bk}}\right)^{k+1}\delta \hat{u}_{bk} + \sum_{a=1}^{n_p} \left(\frac{\partial\Theta_c}{\partial \hat{p}_a}\right)^{k+1}\delta \hat{p}_a \\
&= {}^k\Theta_c + \sum_{b=1}^{n_u} \int_{\Omega} N_c^p N_{b,i}^u d\Omega {}^{k+1}\delta \hat{u}_{bi} + \sum_{a=1}^{n_p} \int_{\Omega} \frac{1}{k} N_c^p N_a^p d\Omega {}^{k+1}\delta \hat{p}_a = 0
\end{aligned} \tag{59}$$

and,

$$\begin{aligned}
{}^{k+1}R_{ij} &\approx {}^kR_{ij} + \left(\frac{\partial R_{ij}}{\partial s_{kl}}\right)^{k+1}\delta s_{kl} + \sum_{a=1}^{n_u} \left(\frac{\partial R_{ij}}{\partial \hat{u}_{ak}}\right)^{k+1}\delta \hat{u}_{ak} \\
&= {}^kR_{ij} - L'_{ijkl} \sum_{a=1}^{n_u} N_{a,l}^u {}^{k+1}\delta \hat{u}_{ak} + \left(I_{ijkl} + 2G\theta\Delta t {}^kC_{ijkl}\right) {}^{k+1}\delta s_{kl} = 0
\end{aligned} \tag{60}$$

in which,

$${}^kC_{ijkl} = \left(\frac{\partial \dot{\epsilon}_{ij}^{vp}}{\partial s_{kl}}\right) \tag{61}$$

The increment of deviatoric stress, ${}^{k+1}\delta s_{ij}$ is evaluated using Eq. 60 as:

$${}^{k+1}\delta s_{ij} = {}^kQ_{ijkl} \left(L'_{klmn} \sum_{a=1}^{n_u} N_{a,n}^u {}^{k+1}\delta \hat{u}_{am} - {}^kR_{kl} \right) \tag{62}$$

where, the modulus ${}^k Q_{ijkl}$ is defined as:

$${}^k Q_{ijkl} = \left(I_{ijkl} + 2G\theta\Delta t {}^k C_{ijkl} \right)^{-1} \quad (63)$$

Substituting Eq. 62 into Eqs. 58 and 59 yields:

$$\begin{aligned} \int_{\Omega} {}^k Q_{ijkl} N_{b,j}^u L'_{klmn} \sum_{a=1}^{n_u} N_{a,n}^u d\Omega^{k+1} \delta \hat{u}_{am} - \sum_{c=1}^{n_p} \int_{\Omega} N_{b,i}^u N_c^p d\Omega^{k+1} \delta \hat{p}_c \\ = \int_{\Omega} {}^k Q_{ijkl} N_{b,j}^u {}^k R_{kl} d\Omega - {}^k \Psi_{bi} \end{aligned} \quad (64)$$

$$- \sum_{b=1}^{n_u} \int_{\Omega} N_c^p N_{b,i}^u d\Omega^{k+1} \delta \hat{u}_{bi} - \sum_{a=1}^{n_p} \int_{\Omega} \frac{1}{k} N_c^p N_a^p d\Omega^{k+1} \delta \hat{p}_a = {}^k \Theta_c \quad (65)$$

When expressed in the matrix form, Eqs. 64 and 65 yield:

$$\begin{bmatrix} {}^k \mathbf{K}^{uu} & \mathbf{K}^{up} \\ (\mathbf{K}^{up})^T & \mathbf{K}^{pp} \end{bmatrix} \begin{Bmatrix} {}^{k+1} \delta \hat{\mathbf{u}} \\ {}^{k+1} \delta \hat{\mathbf{p}} \end{Bmatrix} = \begin{Bmatrix} {}^k \mathbf{f}^u \\ {}^k \mathbf{f}^p \end{Bmatrix} \quad (66)$$

in which,

$${}^k K_{\alpha\beta}^{uu} = \int_{\Omega} N_{b,j}^u {}^k Q_{ijkl} L'_{klmn} N_{a,n}^u d\Omega; \quad \alpha = b + (i-1)n_u; \quad \beta = a + (m-1)n_u \quad (67)$$

$$K_{\alpha c}^{up} = - \int_{\Omega} N_{b,i}^u N_c^p d\Omega; \quad \alpha = a + (i-1)n_u; \quad 1 \leq c \leq n_p \quad (68)$$

$$K_{ab}^{pp} = - \int_{\Omega} \frac{1}{k} N_a^p N_b^p d\Omega; \quad 1 \leq a, b \leq n_p \quad (69)$$

The force vectors are expressed as

$${}^k \mathbf{f}^u = \{ {}^k f_1^u, \dots, {}^k f_{n_{sd} \times n_u}^u \}^T \quad (70)$$

$${}^k \mathbf{f}^p = \{ {}^k f_1^p, \dots, {}^k f_{n_p}^p \}^T \quad (71)$$

and the components of the force vector are given as:

$${}^k f_{\alpha}^u = \int_{\Omega} {}^k Q_{ijkl} N_{b,j}^u {}^k R_{kl} d\Omega - {}^k \Psi_{bi}; \quad \alpha = b + (i-1)n_u \quad (72)$$

$${}^k f_a^p = {}^k \Theta_a; \quad 1 \leq a \leq n_p \quad (73)$$

Based on the definitions above, we employ the following algorithm to compute the pressure and displacement fields:

At $t = 0$, the initial condition of the viscoplastic strain rate is taken as zero, leading to a linear

system of the form:

$$\begin{bmatrix} {}_0\mathbf{K}^{uu} & \mathbf{K}^{up} \\ (\mathbf{K}^{up})^T & \mathbf{K}^{pp} \end{bmatrix} \begin{Bmatrix} {}_0\hat{\mathbf{u}} \\ {}_0\hat{\mathbf{p}} \end{Bmatrix} = \begin{Bmatrix} {}_0\mathbf{f}^u \\ {}_0\mathbf{f}^p \end{Bmatrix} \quad (74)$$

where,

$${}_0K_{\alpha\beta}^{uu} = \int_{\Omega} N_{b,j}^u L'_{ijmn} N_{a,n}^u d\Omega \quad (75)$$

$${}_0f_{\alpha}^u = \int_{\Gamma_N^u} N_b^u \bar{t}_i d\Gamma + \int_{\Omega} N_b^u b_i d\Omega \quad (76)$$

$${}_0f_a^p = - \int_{\Omega} 3N_a^p [\alpha (T - T_0) + \vartheta (c - c_{\infty})] d\Omega \quad (77)$$

The linear system (Eq. 74) is evaluated for the initial state of deformation and pressure coefficients.

At arbitrary time $t + \Delta t$; Given: ${}_t\hat{\mathbf{u}}$, ${}_t\hat{\mathbf{p}}$, ${}_t s_{ij}$ and ${}_t \dot{\varepsilon}_{ij}^{vp}$; Find: ${}_{t+\Delta t}\hat{\mathbf{u}}$, ${}_{t+\Delta t}\hat{\mathbf{p}}$.

1. Initiate the algorithm: $k = 0$.
2. Set the initial guesses of the pressure and deformation coefficients at the current increment:

$${}_0\hat{\mathbf{u}} = {}_t\hat{\mathbf{u}}; \quad {}_0\hat{\mathbf{p}} = {}_t\hat{\mathbf{p}}; \quad {}_0 s_{ij} = {}_t s_{ij}; \quad {}_0 \dot{\varepsilon}_{ij}^{vp} = {}_t \dot{\varepsilon}_{ij}^{vp} \quad (78)$$

3. Loop until convergence:

- (a) Compute the moduli: ${}^k C_{ijkl}$, ${}^k Q_{ijkl}$ using Eqs. 61 and 63, respectively.
- (b) Calculate ${}^k \Psi_{bi}$, ${}^k R_{ij}$, ${}^k \Theta_b$ using Eqs. 54, 57 and 55, respectively.
- (c) Update the pressure and displacement increments, ${}^{k+1}\delta\hat{\mathbf{u}}$ and ${}^{k+1}\delta\hat{\mathbf{p}}$, using Eq. 66.
- (d) Compute deviatoric stress increment ${}^{k+1}\delta s_{ij}$ using Eq. 62.
- (e) Update displacement, pressure and stress:

$${}^{k+1}\hat{\mathbf{u}} = {}^{k+1}\delta\hat{\mathbf{u}} + {}^k\hat{\mathbf{u}} \quad (79)$$

$${}^{k+1}\hat{\mathbf{p}} = {}^{k+1}\delta\hat{\mathbf{p}} + {}^k\hat{\mathbf{p}} \quad (80)$$

$${}^{k+1}s_{ij} = {}^{k+1}\delta s_{ij} + {}^k s_{ij} \quad (81)$$

- (f) Update ${}^{k+1}\dot{\varepsilon}_{ij}^{vp}$ and ${}^{k+1}\varepsilon_{ij}^{vp}$ by simultaneously evaluating:

$${}^{k+1}\varepsilon_{ij}^{vp} = {}_t\varepsilon_{ij}^{vp} + \theta\Delta t {}^{k+1}\dot{\varepsilon}_{ij}^{vp} + (1 - \theta)\Delta t {}_t\dot{\varepsilon}_{ij}^{vp} \quad (82)$$

$${}^{k+1}\dot{\varepsilon}_{ij}^{vp} = \gamma \left\langle \frac{{}^{k+1}f}{{}^{k+1}\sigma_Y} \right\rangle^q {}^{k+1} \left(\frac{\partial f}{\partial \sigma_{ij}} \right) \quad (83)$$

- (g) $k = k + 1$

Table 1: Material parameters for viscoplastic deformation of Ti-6Al-2Sn-4Zr-2Mo-0.1Si.

ν	E_0 [GPa]	γ [MPa/s]	q	α [1/°C]	ϑ [1/%c]
0.32	120.8	25.0	1.0	7.7e-6	1.1e-3
A [MPa]	B [MPa]	F [MPa/%c]	n	m	c_{crit} [%]
895.0	125.0	140.0	0.2	0.85	4.5
T_{melt} [°C]	$\dot{\epsilon}^0$ [1/s]	D_1^∞	D_1^α	D_5	
1700.0	1.0	0.1676	5.0e-3	3.0	

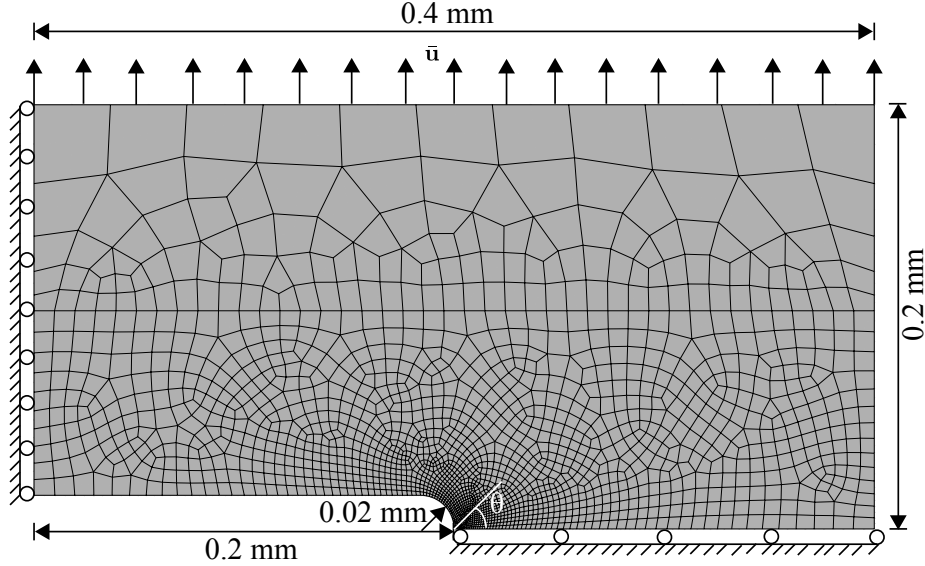


Figure 3: Geometry, boundary conditions and the finite element mesh of the notched specimen.

4 Numerical Verification

In this section, the performance of the proposed three-field model is verified using numerical simulations. The effect of element type on the accuracy and stability characteristics of the transport and deformation problems based on numerical simulations is investigated.

We are concerned with the response of a near alpha titanium alloy, Ti-6Al-2Sn-4Zr-2Mo-0.1Si (Ti-6242S), which displays good mechanical properties at high temperatures. When exposed to high temperatures for an extended period of time, this alloy is known to exhibit significant embrittlement [5] caused by ingress of oxygen. The material properties that characterize the mechanical response at a wide range of temperatures and oxygen exposure are summarized in Table 1. Figure 3 illustrates the geometry and discretization of the numerical specimen. The specimen dimensions are 0.8mm x 0.4mm with a 0.4mm deep notch at the middle. The notch radius is $20\mu\text{m}$. Due to symmetry, only a quarter of the specimen is discretized (with 1846 quadrilateral elements or 3298 triangular elements). The notched specimen is employed to generate a stress gradient, which captures the effects of advection and reaction terms in the transport model. Plane strain conditions are assumed.

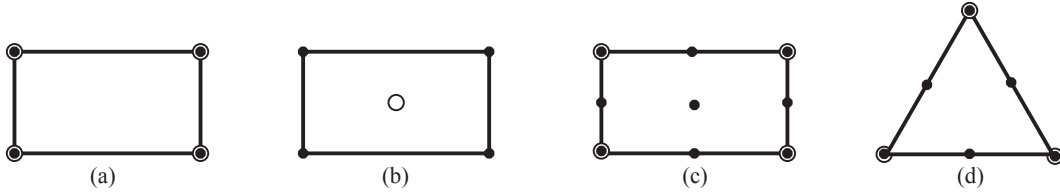


Figure 4: The nodal positions in the mixed finite elements: (a) u4p4; (b) u4p1; (c) u9p4 and (d) u6p3.

The specimen is discretized using four types of elements, named as u4p4, u4p1, u6p3 and u9p4. The types of elements and the associated nodal positions are shown in Fig. 4. u4p4 consists of four-noded Lagrangian quadrilateral elements for both displacement and pressure degrees of freedom. In u4p1, the pressure is discretized using a single node positioned at the centroid of the finite element, whereas the displacement is discretized using four-node quadrilateral elements. Two types of Taylor-Hood elements were employed. u6p3 consists of a triangular, quadratic, six-node element for displacement degrees of freedom, and a three-node, linear element for pressure degrees of freedom. u9p4 consists of a quadrilateral, bi-quadratic, nine-node Lagrangian element for displacement degrees of freedom, whereas a four-node bi-linear element is employed for pressure degrees of freedom. In u4p4, u6p3 and u9p4 elements, the pressure field exhibits inter-element continuity, allowing a straightforward computation of the pressure gradients (i.e., using Eq. 53). In all four element types, the displacement discretization is isoparametric, whereas pressure field is non-isoparametric. The performance of the four mixed elements are compared to the reference model (denoted as u4), which is the standard displacement-based finite element with four-noded bi-linear shape functions. In u4, the pressure is evaluated at the integration points.

In the case of u4p1 element, the pressure is constant within a finite element, and Eq. 53 cannot be used to directly compute the pressure gradients. The computation of the pressure gradient for u4p1 is based on the pressure smoothing procedure of the least squares type [17]. In this procedure, a piecewise continuous smoothed pressure field is computed. The smoothed pressure approximation is made as a function of four-noded bilinear Lagrangian quadrilateral shape functions. The pressure gradient is then computed using Eq. 53 from the smoothed pressure field.

The specimen is subjected to displacement controlled tensile loading with maximum amplitude of $6.4e^{-4}$ mm applied in 11.52 seconds at 650°C and the mechanical response is evaluated using the four mixed elements described above. Figures 5 and 6 display the pressure as a function of distance from the notch tip plotted along lines 0° and 70° to the horizontal, respectively. The pressure profiles at the loading magnitudes of $4.32e^{-4}$ mm and $6.32e^{-4}$ mm are shown. At both loading amplitudes a zone of plastic deformation forms around the notch tip as shown in Fig. 7. The peak pressure moves away from the notch tip as the loading increases due to accumulation of damage and expansion of the area of the plastic zone. All four models

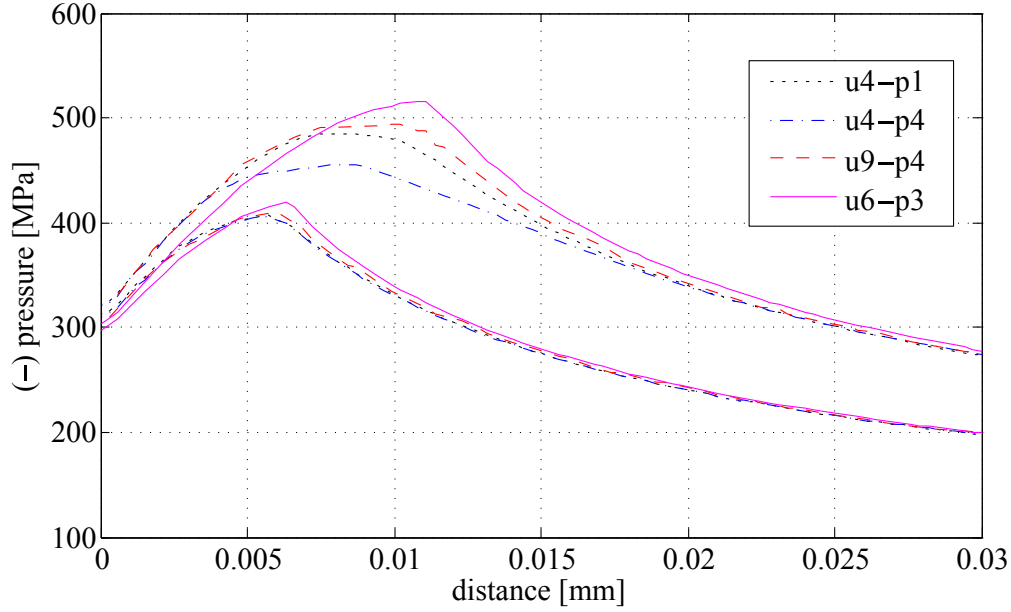


Figure 5: Pressure distribution along the notch tip: $\theta = 0$.

yield similar response at low loading amplitude, but the results begin to deviate as the loading increases. u4p4 displays slight oscillation around the peak pressure (Fig. 6), whereas u4p1, u6p3 and u9p4 elements yield response free of oscillations. The pressure predictions of u4p1, u6p3 and u9p4 are stable everywhere inside the problem domain and in reasonable agreement throughout the loading history. For u4p4 element, the pressure oscillations are observed within part of the specimen domain and it is severe along the 70° to the horizontal. Figure 8 shows the oscillating pressure distribution around the notch tip at the loading magnitudes of $4.32e^{-4}$ mm and $6.32e^{-4}$ mm. The oscillatory behavior of the u4p4 element is expected as this element does not satisfy the Babuska-Brezzi stability criteria and therefore not guaranteed to be stable.

The convergence characteristics of the mixed formulation are investigated in a mesh sensitivity study. The mesh sensitivity study was performed using the u6p3 elements. The pressure variations around the notch tip at $\Theta = 0$ orientation computed using three different mesh densities are shown in Fig. 9. The results correspond to the applied magnitudes of $4.32e^{-4}$ mm (lower curves) and $6.32e^{-4}$ mm (upper curves). In the three discretizations considered, the element edge lengths around the crack tip were set to $h = 2 \mu\text{m}$, $1 \mu\text{m}$ and $0.5 \mu\text{m}$, respectively. All three mesh densities produce very similar pressure profiles. The pressure profiles computed using the $h = 0.5 \mu\text{m}$ and $1 \mu\text{m}$ edge lengths are nearly identical, pointing to mesh convergence.

The key benefit of employing the mixed finite element approach in computing the coupled aggressive agent ingress and deformation response is to accurately capture the pressure gradients across the problem domain. The pressure gradient fields are in turn employed in accurately capturing the transport response. This is in contrast to the displacement-based finite element method, in which the stresses are computed point-wise at the integration points and

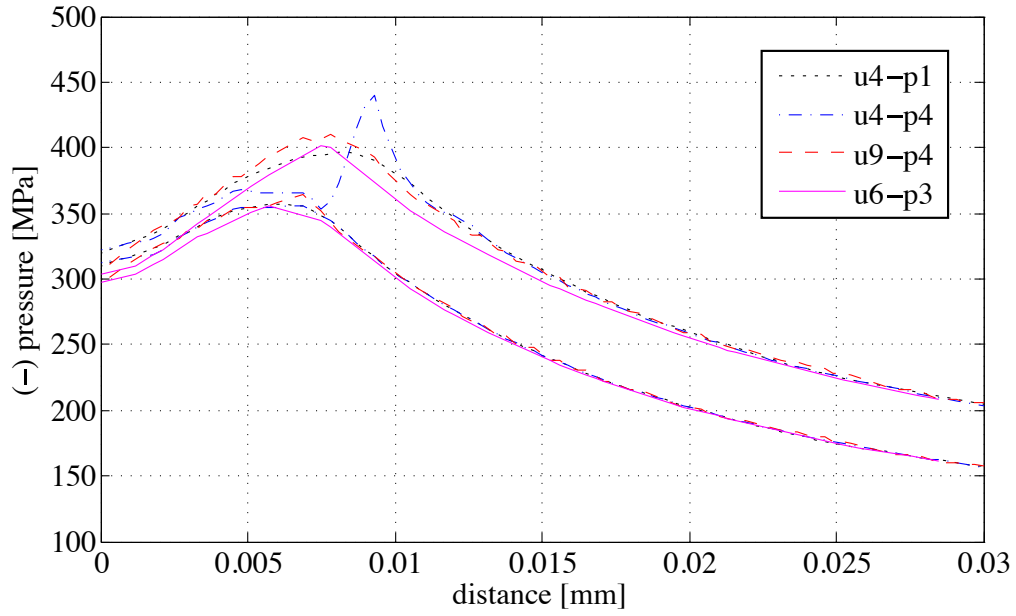


Figure 6: Pressure distribution along the notch tip: $\theta = 70$.

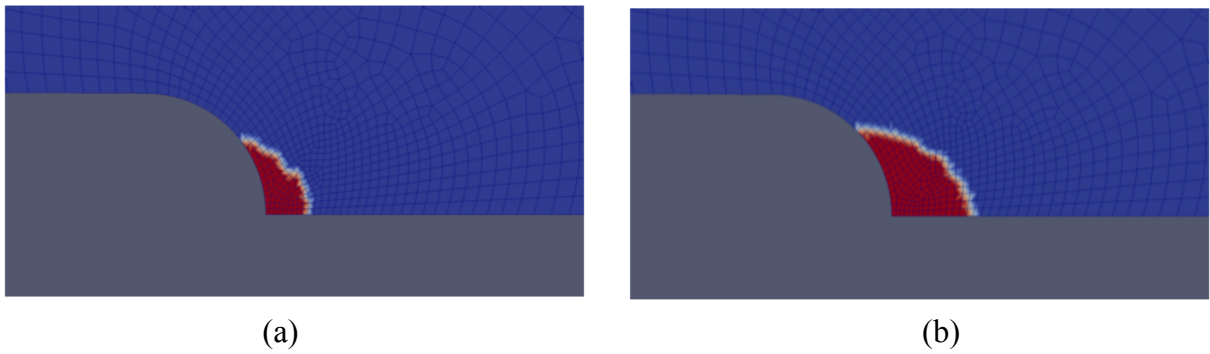


Figure 7: The area of plastic deformation at applied displacement: (a) $4.32e^{-4}$ mm ; (b) $6.32e^{-4}$ mm computed using the u9p4 model.

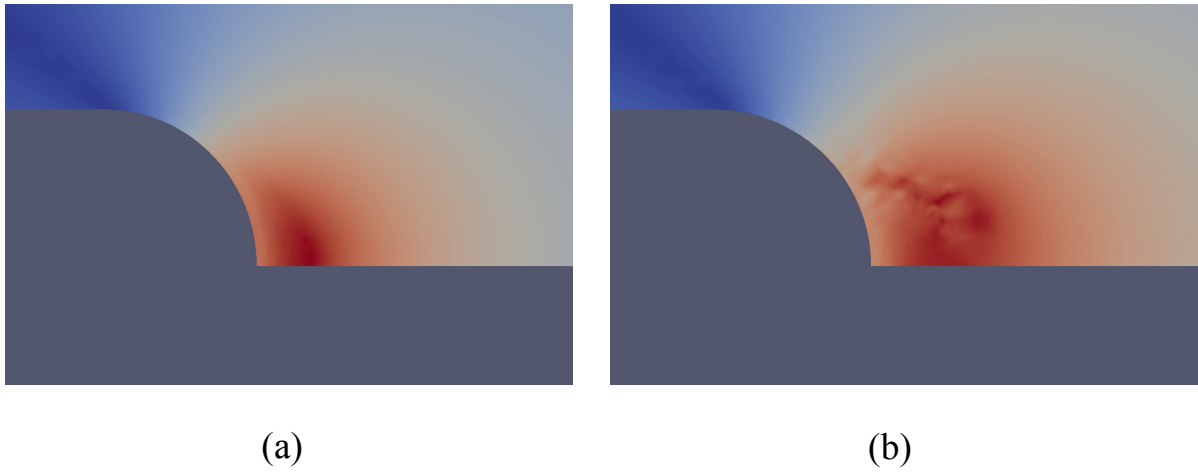


Figure 8: The pressure field at applied displacement: (a) $4.32e^{-4}$ mm ; (b) $6.32e^{-4}$ mm computed using the u4p4 model.

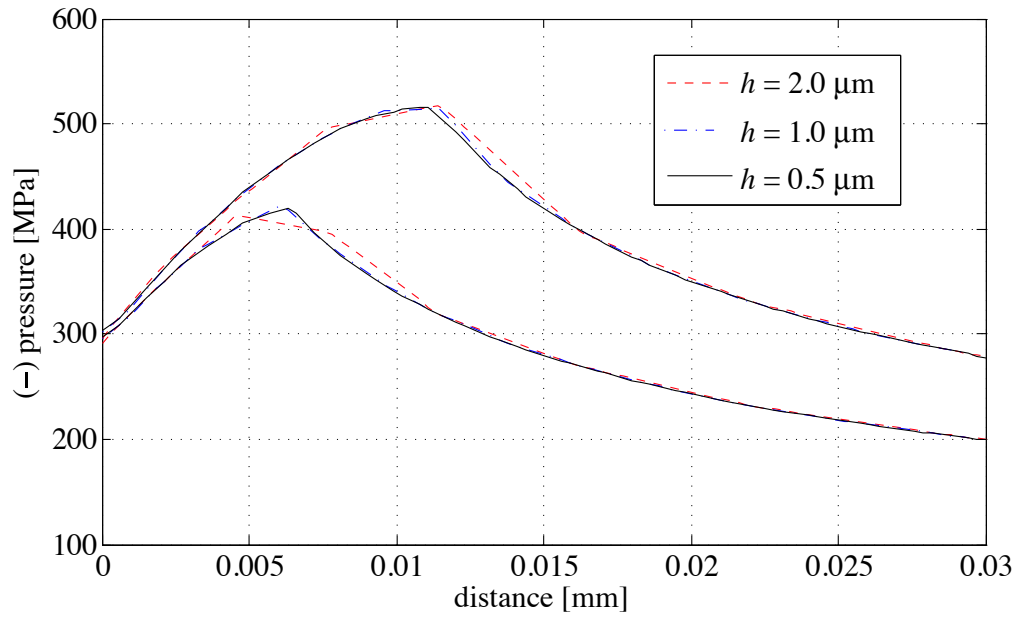


Figure 9: The pressure distributions along the notch tip ($\theta = 0$ direction) computed using the u6p3 elements with element edge lengths of $2\mu\text{m}$, $1\mu\text{m}$ and $0.5\mu\text{m}$.

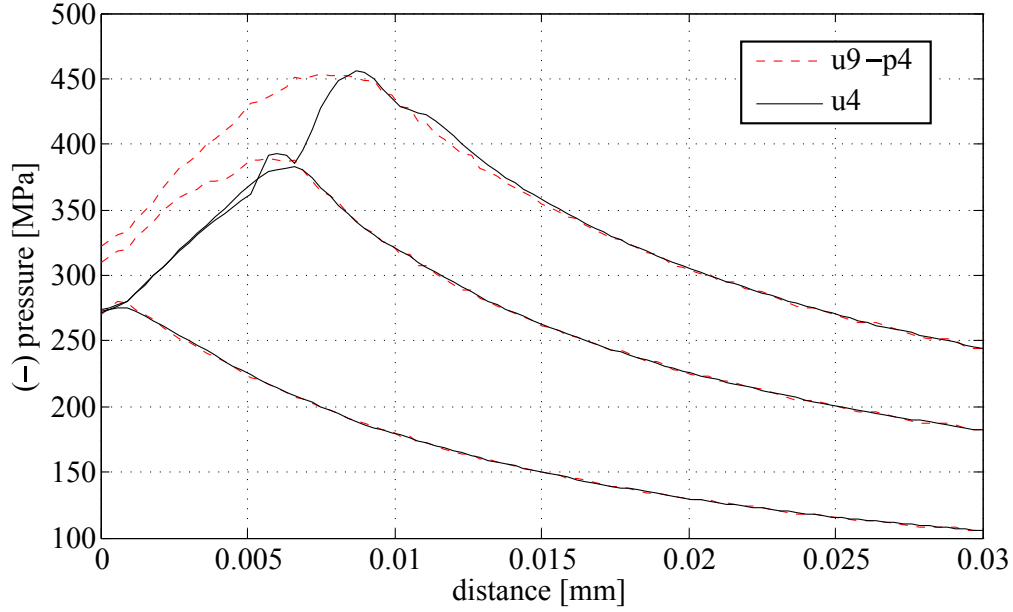


Figure 10: Pressure distribution along the notch tip: $\theta = 45$.

must be approximated to extract the pressure gradient fields. It is convenient and accurate to use the mixed approach since the pressure is available as a continuous field. Additionally, the mixed finite element method addresses the well-known numerical issues related to incompressible materials and incompressible flow within the plastic deformation process. Figure 10 shows the pressure distributions as a function of distance from the notch tip plotted along the direction 45° to the horizontal at loading magnitudes of $1.84e^{-4}$ mm, $4.32e^{-4}$ mm and $6.32e^{-4}$ mm, respectively. The pressure distributions computed using the u9p4 and u4 models are compared. The pressure profile of the u4 model is obtained by interpolating the point-wise pressure values at the integration and smoothing the interpolated response. When the applied loading is low and the accumulated plastic strains are small, the pressure distributions from the displacement-based and mixed formulations are very similar. At higher loading amplitudes, significant discrepancy is observed between the mixed and displacement-based formulations close to the notch tip. The mixed formulation also results in a relatively smooth pressure field as a function of distance from the notch tip compared to the displacement-based formulation, which displayed some oscillations. Away from the notch tip, where the pressure gradients are low, the pressure plots from the mixed- and displacement-based formulations are very similar.

Next, the performance of the proposed stabilized transport model is investigated in the context of a mechanical pressure dependent oxygen transport problem. The numerical specimen is heated to a uniform temperature of 650°C and kept at this constant temperature level for the duration of 420 hours. The time step size employed in the simulations below is set to 1 hour. The nonuniform pressure field computed in the example above is employed in the simulations. The pressure field is taken to be time-invariant throughout the duration of the simulation. While, stress relaxation would likely occur at such high temperatures, the pressure field is set

Table 2: Material parameters for oxygen transport in Ti-6Al-2Sn-4Zr-2Mo-0.1Si.

D_0 [mm ² /sec]	c_∞ [%]	Q [KJ/mole]	ω_c	ω_{ec}	a	\bar{V}_O [cm ³ /mole]
5.39	0.15	184.0	0.1	0.7	3.56	3.5

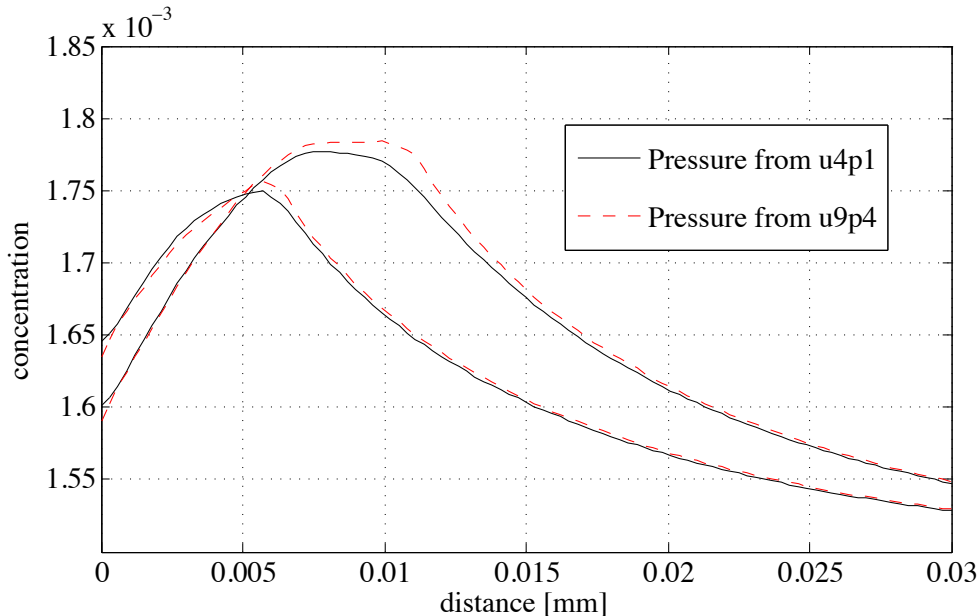


Figure 11: Concentration distribution along the notch tip: $\theta = 0$.

as constant (but spatially non-uniform) to assess the performance of the transport model in the presence of significant pressure gradient fields. The transport properties that control the oxygen ingress process into the titanium alloy are summarized in Table 2. The diffusivity is taken to be independent of concentration magnitude. In the transport simulations, no external boundary concentrations or boundary fluxes are imposed, and the transport is taken to be due to pressure gradient induced internal advection only. The pressure induced oxygen transport within the specimen is observed for the duration of high temperature exposure. The transport problem is discretized using four-node bi-linear elements for concentration degrees of freedom. Figure 11 displays the oxygen concentration profiles obtained by the transport model plotted as a function of distance from the notch tip along the horizontal line (i.e., $\theta = 0$). The two plots compare the concentration profiles computed using the pressures from u4p1 and u4p9 deformation models. Elevated pressures lead to increased advection flow of oxygen and higher oxygen concentrations. The concentration profiles computed using the pressures from u4p1 and u9p4 models are close to each other and computation of the pressure fields using both models provide reasonable approximations.

In order to verify the stabilization scheme employed in the transport model, a parametric study is performed by varying the Peclet number of the transport equation. The Peclet number (i.e., Eq. 41) controls the contribution of the advection component of the transport with

respect to the diffusion component. At high Peclet numbers, unstabilized transport models exhibit instability and inaccuracy. For all simulations in the parametric study, the pressure profile computed using the u9p4 deformation model is employed. Figures 12-14 compares the oxygen concentration fields generated using the stabilized and unstabilized transport models. The normalized concentration fields are plotted along the horizontal line ($\theta = 0$) from the notch tip. Figures 12, 13 and 14 shows simulations conducted using the value of the Peclet numbers of $P_e = 1.52 \times 10^{-4} \|p_{,i}\| h_e$; $1.52 \times 10^{-2} \|p_{,i}\| h_e$ and $6.08 \times 10^{-2} \|p_{,i}\| h_e$; respectively, the former computed by the material parameters shown in Table 2. The exact value of the Peclet number varies as a function of the pressure gradient as well as the characteristic size of the element. The Peclet numbers are achieved by varying the coefficient of advection, α . When the original Peclet number is employed, the stabilized and the unstabilized simulations coincide, indicating that the transport is diffusion dominated. For increased values of the Peclet numbers, the unstabilized model exhibits significant errors. When the Peclet number is equal to $1.52 \times 10^{-2} \|p_{,i}\| h_e$, significant deviations in the concentration values between the stabilized and unstabilized simulations are observed. When the Peclet number is set to $6.08 \times 10^{-2} \|p_{,i}\| h_e$, severe oscillations are generated by the unstabilized model with negative concentration values. In all cases considered, the stabilized model displays concentration distribution free of oscillations around the notch tip. The present parametric study artificially varied the Peclet number to investigate the stability of the proposed transport model and instability was only observed when the Peclet number is set to a higher than the original value. There exists a significant variability in the transport parameters measured even in a single alloy type [18], which contributes to wide variations in the Peclet numbers. In addition, the presence of high thermal gradients and cracks may also lead to high advection coefficients and high Peclet number transport.

5 Conclusion

This manuscript provided a three-field computational model for coupled transport-deformation problems. The proposed model is based on a tightly coupled two-field formulation for the viscoplastic deformation response to provide accurate pressure and pressure gradient fields to a transport problem. It is demonstrated that modeling the transport processes at the high stress gradient zones such as around notch tips requires accurately approximating the pressure and pressure gradient fields. The proposed computational model conveniently and accurately computes these fields based on the mixed finite element approach.

A number of challenges remain to be investigated in predictive modeling of transport-deformation problems. One of the main challenges is because of the localized character of the transport process. In some practical problems, the oxygen ingress is localized within a very small boundary region of the structure with a thickness of the order of a few grain diameters. Accurate characterization of localized deformation and failure within this zone necessitates

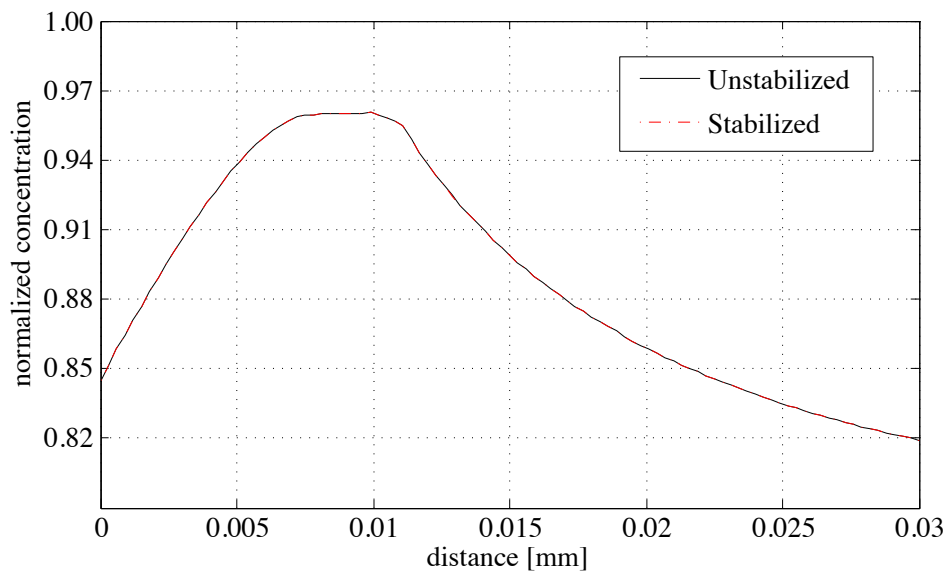


Figure 12: Normalized concentration distribution along the notch tip: $\theta = 0$ computed using the $P_e = 1.52 \times 10^{-4} \|p_i\| h_e$.

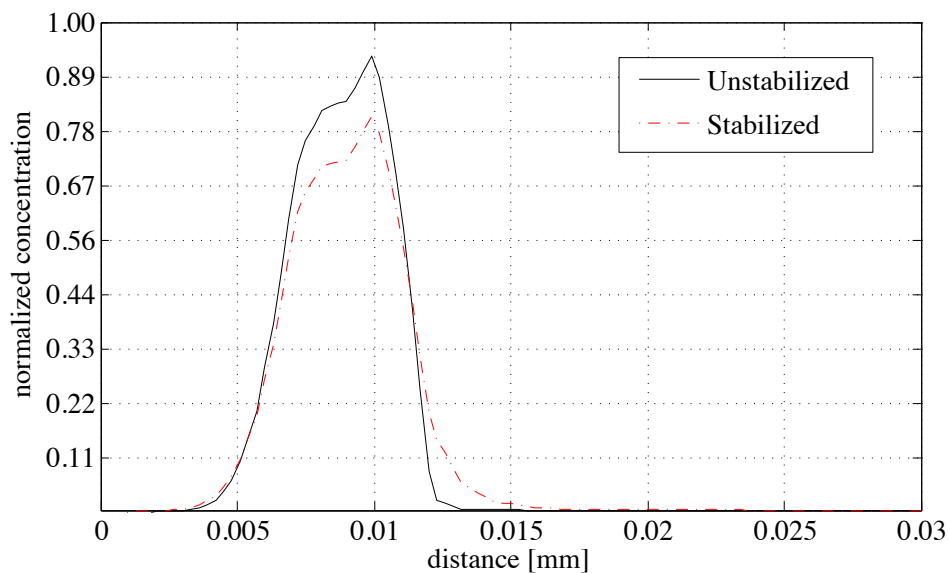


Figure 13: Normalized concentration distribution along the notch tip: $\theta = 0$ computed using the $P_e = 1.52 \times 10^{-2} \|p_i\| h_e$.

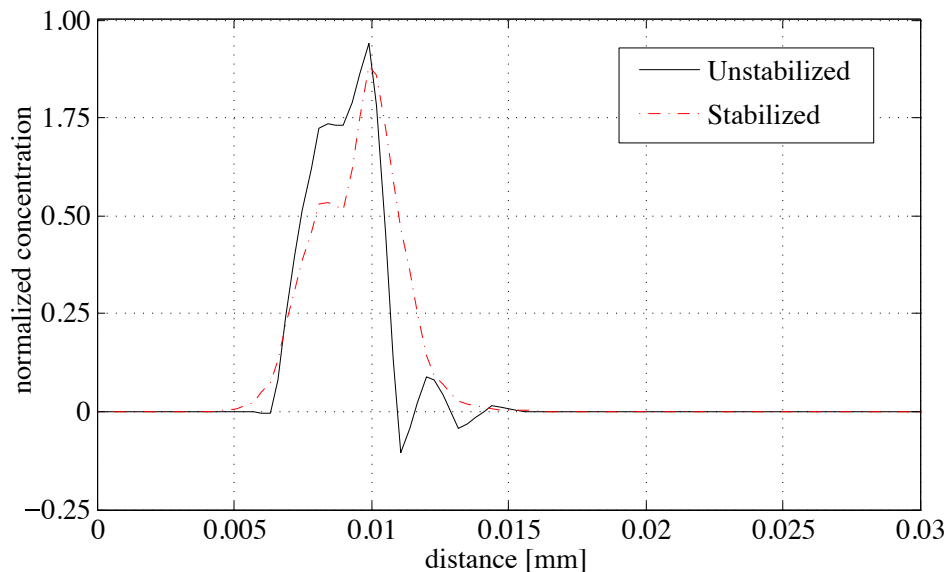


Figure 14: Normalized concentration distribution along the notch tip: $\theta = 0$ computed using the $P_e = 6.08 \times 10^{-2} \|p_i\| h_e$.

resolution of the grain scale deformation and transport processes within the boundary region. Multiscale computational models that can accurately incorporate such grain scale information into a structural scale problem remain an outstanding issue. Such models are currently under investigation [19] and will be employed to address localized coupled transport - inelastic deformation problems.

6 Acknowledgements

The authors gratefully acknowledge the financial and technical support from the Air Force Research Laboratory, Structural Sciences Center (Contract No: GS04T09DBC0017 through High Performance Technologies, Inc.) and the Air Force Office of Scientific Research Multi-Scale Structural Mechanics and Prognosis Program (Grant No: FA9550-13-1-0104). Program Manager: Dr. David Stargel.

References

- [1] T. Ericsson. Review of oxidation effects on cyclic life at elevated temperature. *Can. Metall. Quart.*, 18:177–195, 1979.
- [2] R. A. Oriani, J. P. Hirth, and M. Smailowski, editors. *Hydrogen degradation of ferrous alloys*. Noyes Publications, Park Ridge, USA, 1985.

- [3] P. Sofronis and R. M. McMeeking. Numerical analysis of hydrogen transport near a blunt crack tip. *J. Mech. Phys. Solids*, 37:317–350, 1989.
- [4] M. J. Donachie. *Titanium: A Technical Guide*. ASM International, 2nd edition, 2000.
- [5] C. Leyens and M. Peters. *Titanium and Titanium Alloys*. Wiley-VCH, 2003.
- [6] C. Oskay and M. Haney. Computational modeling of titanium structures subjected to thermo-chemo-mechanical environment. *Int. J. Solids Struct.*, 47:3341–3351, 2010.
- [7] A. H. M. Krom, R. W. J. Koers, and A. Bakker. Hydrogen transport near a blunting crack tip. *J. Mech. Phys. Solids*, 47(4):971–992, April 1999.
- [8] S. Ndong-Mefane, H. Kanayama, and M. F. Oginio, M. El-Amin. A stabilization method for the hydrogen diffusion model in materials. *J. Comput. Sci. Technol.*, 2:447–458, 2008.
- [9] J. C. M Li, R. A. Oriani, and L. S. Darken. Thermodynamics of stressed solids. *Zeitschrift Fur Physikalische Chemie-Frankfurt*, 49(3-5):271, 1966.
- [10] A. L. Ruoff and R. W. Balluffi. On strain enhanced diffusion in metals. iii. Interpretation of recent experiments. *J. Appl. Phys.*, 34:2862–2872, 1963.
- [11] R. L. Salganik. Transport processes in bodies with a large number of cracks. *Journal of Engineering Physics and Thermophysics*, 27(1534-1538), 1974.
- [12] D. Krajcinovic, M. Basista, K. Mallick, and D. Sumarac. Chemo-micromechanics of brittle solids. *J. Mech. Phys. Solids*, 40:965–990, 1992.
- [13] S. Kirkpatrick. Percolation and conduction. *Rev. Mod. Phys.*, 45:574–588, 1973.
- [14] L. P. Franca, H. Guillermo, and A. Masud. Revisiting stabilized finite element methods for the advective–diffusive equation. *Comput. Methods Appl. Mech. Engrg.*, 195:1560–1572, 2006.
- [15] L. P. Franca, S. L. Frey, and T. J. R. Hughes. Stabilized finite element methods: I. Application to the advective-diffusive model. *Comput. Methods Appl. Mech. Engrg.*, 95:253–276, 1992.
- [16] H. P. Langtangen. *Computational Partial Differential Equations: Numerical Methods and Diffpack Programming*. Springer, 2003.
- [17] T. J. R. Hughes, W. K. Liu, and A. Brooks. Finite element analysis of incompressible viscous flows by the penalty function formulation. *J. Comput. Phys.*, 30:1–60, 1979.
- [18] Z. Liu and G. Welsch. Literature survey on diffusivities of oxygen, aluminum and vanadium in alpha titanium, beta titanium, and in rutile. *Metall. Trans. A*, 19:1121–1125, 1988.

- [19] C. Oskay. Variational multiscale enrichment for modeling coupled mechano-diffusion problems. *Int. J. Numer. Meth. Engng.*, 89:686–705, 2012.